ISSN 1674-1056
http://cpb.iphy.ac.cn
http://iopscience.iop.org/cpb
中国物理 B
Chinese Physics
中国物理 Chinese Physics B

Growth of high-quality perovskite (110)-$SrIrO_3$ thin films using reactive molecular beam epitaxy

Kai-Li Zhang(张凯莉), Cong-Cong Fan(樊聪聪), Wan-Ling Liu(刘万领), Yu-Feng Wu(吴宇峰), Xiang-Le Lu(卢祥乐), Zheng-Tai Liu(刘正太), Ji-Shan Liu(刘吉山), Zhong-Hao Liu(刘中灏), Da-Wei Shen(沈大伟)

Citation: Chin. Phys. B . 2018, 27(8): 088103. **doi:** 10.1088/1674-1056/27/8/088103

Journal homepage: http://cpb.iphy.ac.cn; http://iopscience.iop.org/cpb

What follows is a list of articles you may be interested in

Effects of growth conditions on optical quality and surface morphology of InGaAsBi

Jia-Kai Li(李家恺), Li-Kun Ai(艾立鹍), Ming Qi(齐鸣), An-Hui Xu(徐安怀), Shu-Min Wang(王庶民)
Chin. Phys. B . 2018, 27(4): 048101. **doi:** 10.1088/1674-1056/27/4/048101

Effect of substrate curvature on thickness distribution of polydimethylsiloxane thin film in spin coating process

Ying Yan(闫英), Ping Zhou(周平), Shang-Xiong Zhang(张尚雄), Xiao-Guang Guo(郭晓光), Dong-Ming Guo(郭东明)
Chin. Phys. B . 2018, 27(6): 068104. **doi:** 10.1088/1674-1056/27/6/068104

Influences of substrate temperature on microstructure and corrosion behavior of APS $Ni_{50}Ti_{25}Al_{25}$inter-metallic coating

Sh Khandanjou, M Ghoranneviss, Sh Saviz, M Reza Afshar
Chin. Phys. B . 2018, 27(2): 028104. **doi:** 10.1088/1674-1056/27/2/028104

Preparation and characterization of PTFE coating in new polymer quartz piezoelectric crystal sensor for testing liquor products

Gu Yu, Li Qiang
Chin. Phys. B . 2015, 24(7): 078106. **doi:** 10.1088/1674-1056/24/7/078106

Quantum dots-templated growth of strain-relaxed GaN on a *c*-plane sapphire by radio-frequency molecular beam epitaxy

Guo Hao-Min, Wen Long, Zhao Zhi-Fei, Bu Shao-Jiang, Li Xin-Hua, Wang Yu-Qi
Chin. Phys. B . 2012, 21(10): 108101. **doi:** 10.1088/1674-1056/21/10/108101

Growth of high-quality perovskite (110)-$SrIrO_3$ thin films using reactive molecular beam epitaxy

Kai-Li Zhang(张凯莉)[1,2,†], Cong-Cong Fan(樊聪聪)[1,2,†], Wan-Ling Liu(刘万领)[3], Yu-Feng Wu(吴宇峰)[1,2], Xiang-Le Lu(卢祥乐)[1,2], Zheng-Tai Liu(刘正太)[1,4], Ji-Shan Liu(刘吉山)[1,4], Zhong-Hao Liu(刘中灏)[1,4], and Da-Wei Shen(沈大伟)[1,4,‡]

[1] *State Key Laboratory of Functional Materials for Informatics, Shanghai Institute of Microsystem and Information Technology (SIMIT), Chinese Academy of Sciences (CAS), Shanghai* 200050, *China*

[2] *University of Chinese Academy of Sciences, Beijing* 100049, *China*

[3] *School of Physical Science and Technology, ShanghaiTech University, Shanghai* 200031, *China*

[4] *CAS Center for Excellence in Superconducting Electronics (CENSE), Shanghai* 200050, *China*

(Received 1 May 2018; revised manuscript received 20 May 2018; published online 10 July 2018)

Recently, 5d transition metal iridates have been reported as promising materials for the manufacture of exotic quantum states. Apart from the semimetallic ground states that have been observed, perovskite $SrIrO_3$ is also predicted to have a lattice-symmetrically protected topological state in the (110) plane due to its strong spin–orbit coupling and electron correlation. Compared with non-polar (001)-$SrIrO_3$, the especial polarity of (110)-$SrIrO_3$ undoubtedly adds the difficulty of fabrication and largely impedes the research on its surface states. Here, we have successfully synthesized high-quality (110)-$SrIrO_3$ thin films on (110)-$SrTiO_3$ substrates by reactive molecular beam epitaxy for the first time. Both reflection high-energy electron diffraction patterns and x-ray diffraction measurements suggest the expected orientation and outstanding crystallinity. A (1×2) surface reconstruction driven from the surface instability, the same as that reported in (110)-$SrTiO_3$, is observed. The electric transport measurements uncover that (110)-$SrIrO_3$ exhibits a more prominent semimetallic property in comparison to (001)-$SrIrO_3$.

Keywords: molecular beam epitaxy, iridates, topological crystalline metal, surface reconstruction

PACS: 81.15.–z, 61.05.jh, 71.70.Ej, 71.27.+a **DOI:** 10.1088/1674-1056/27/8/088103

1. Introduction

The co-existence of strong spin–orbit coupling (SOC) and electron–electron correlations has triggered numerous novel quantum states in 5d transition metal iridates.[1–7] Among perovskite iridates, the $n = \infty$ end-member $SrIrO_3$ of the Ruddlesden–Popper series $Sr_{n+1}Ir_nO_{3n+1}$, has attracted growing attention due to its possible exotic topological phases.[8–14] *In situ* angle-resolved photoemission spectroscopy (ARPES) measurements have unveiled a Dirac cone in the bulk state of epitaxially grown (001)-$SrIrO_3$ films,[8,9] which is reminiscent of a symmetry-protected nodal line predicted by theoretical calculations.[11,12] Furthermore, a recent theoretical work based on the tight-binding model predicted that orthorhombic perovskite $SrIrO_3$ is a potential topological crystalline metal with zero-energy surface states protected by the mirror-reflection symmetry in the (110) plane.[15] However, although the synthesis of (001)-$SrIrO_3$ using both pulsed laser deposition (PLD)[16] and reactive molecular beam epitaxy (MBE) techniques[8,9] have been widely reported, the epitaxial growth of (110)-$SrIrO_3$ thin films still suffers from severe technical barriers, and films of both high crystalline and surface quality are sill lacking, which is actually the prerequisite for further verifying its topological non-triviality.

In this work, we comprehensively investigate the synthesis process of (110)-$SrIrO_3$ thin films by reactive MBE and overcome the difficulty in the preparation of such polar multicomponent oxides. *In situ* reflection high-energy electron diffraction (RHEED) monitoring and *ex situ* x-ray diffraction (XRD) test both demonstrate the desired [110] orientation of the $SrIrO_3$ films as well as the high-quality crystallization. In addition, by comparing with the [001]-oriented counterpart using electrical transport measurements, (110)-$SrIrO_3$ exhibits more pronounced semimetallic behavior at temperatures from 2 K to 300 K.

2. Experiment

Reactive MBE is considered to be the most significant growth method for perovskite oxides to date, providing ultra-high orientation and pure phase as well as atomic-level flat-

*Project supported by the National Key Research and Development Program of the MOST of China (Grant No. 2016YFA0300204), the National Key Basic Research Program of China (Grant No. 2015CB654901), the National Natural Science Foundation of China (Grant Nos. 11574337, 11227902, 11474147, and 11704394), Shanghai Sailing Program (Grant No. 17YF1422900), and the Award for Outstanding Member in Youth Innovation Promotion Association of the Chinese Academy of Sciences.

†These authors contributed equally.

‡Corresponding author. E-mail: dwshen@mail.sim.ac.cn

© 2018 Chinese Physical Society and IOP Publishing Ltd

ness. (110)-$SrIrO_3$ were epitaxially grown on (110)-$SrTiO_3$ substrates by co-deposition mode, which follows the thermodynamics mechanism[17] and can automatically control the composition with all elements' shutters being open during the growth process. In general, commercial substrates tend to undergo some pretreatments before film growth. Here, the mixed cut-off (110)-$SrTiO_3$ substrate was ultrasonically cleaned with acetone and dehydrated ethanol for 10 minutes each in the atmosphere, then transfered into a loadlock chamber with 200 °C heating for more than 2 hours to obtain a clean surface. In the growth chamber, under a distilled O_3 background pressure of 2.5×10^{-6} Torr (1 Torr = 1.33322×10^2 Pa), the substrate temperature was set to 650 °C. It is worth noting that once the substrate temperature is higher than 300 °C, a continuous oxidizing agent is needed to compensate for the oxygen loss of the substrate. Strontium and iridium atoms were respectively evaporated from a low-temperature effusion cell and electron beam evaporator with a precise flux ratio of 1:1 measured by a quartz crystal microbalance.

Perovskite $SrIrO_3$ (*Pbnm*) can be seen in the [001] direction as alternating layers of electrically neutral $(SrO)^0$ and $(IrO_2)^0$ with the layer spacing of $a/2 = 1.98$ Å, making (001)-$SrIrO_3$ a non-polar oxide. On the contrary, (110)-$SrIrO_3$ is identified as a polar oxide due to the stacks of oppositely charged layers $(SrIrO)^{4+}$ and $(O_2)^{4-}$ [Fig. 1(c)], which are seperated by $a/2\sqrt{2} = 1.40$ Å. If a non-polar substrate is utilized to grow a polar film, the intrinsic polarity discontinuity of these two materials will induce polarity catastrophes,[18,19] directly affecting the nucleation in the initial growth period and leading to complicated unexpected reconstruction. As a result, the interface and surface of the film become quite rough and multiphase co-existence occurs. The lattice constants of $SrTiO_3$ and $SrIrO_3$ along $[1\bar{1}0]$ are 5.52 Å and 5.60 Å, respectively. Therefore, under the premise of minimizing lattice mismatch (1.4%), we consider the polar (110)-$SrTiO_3$ as the substrate to eliminate polarity catastrophes. In order to improve the interface flatness, homo-epitaxial 20-unit-cell (20 u.c.) $SrTiO_3$ buffer layers were deposited first [Fig. 1(b)].

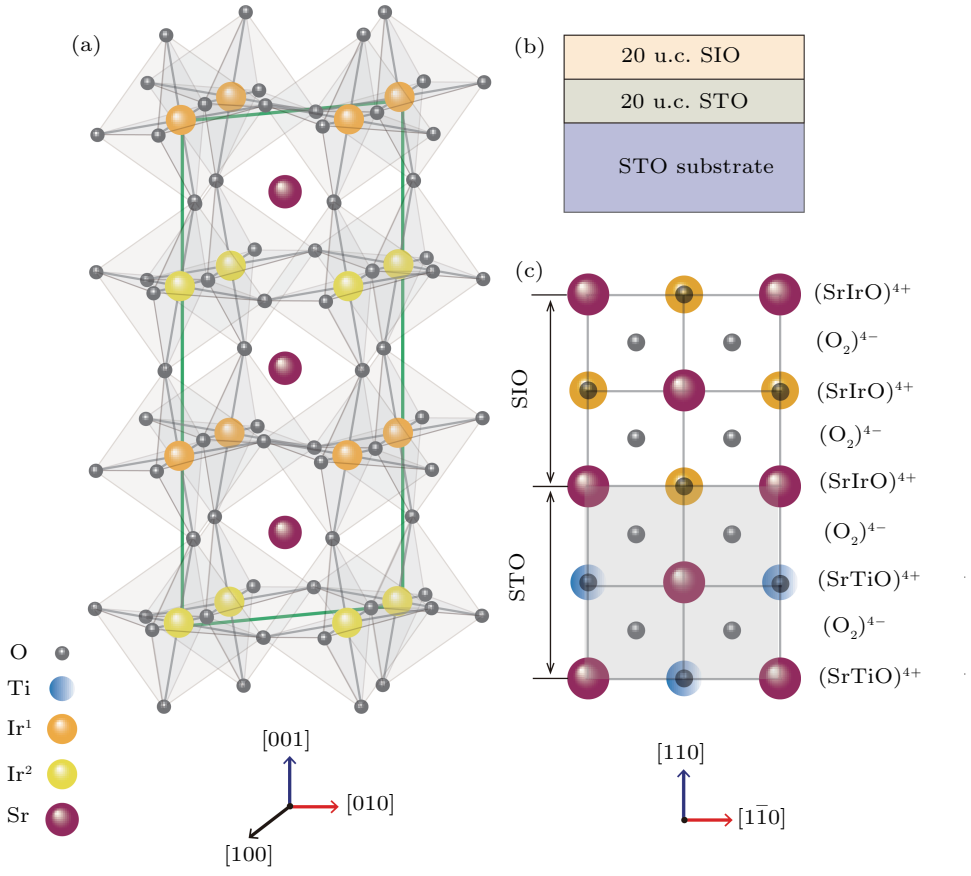


Fig. 1. (color online) (a) Crystal structure of perovskite $SrIrO_3$. (b) Schematic view of the as-synthesized heterostructure. (c) Schematic diagram of interface polarity between the $SrTiO_3$ buffer layer and $SrIrO_3$ along the [110] direction.

3. Results and discussion

Figures 2(a)–2(c) show *in-situ* RHEED monitoring of the growth process. With the deposition of buffer layers, the intensity of (01) diffraction spot of (110)-$SrTiO_3$ substrate gradually increases, at the same time, another diffraction spot (02) appears (marked with a blue square), which indicates that the possible grooves on the surface of the substrate have already been filled, laying a strong foundation for subsequent high-quality film growth. It is worth noting that once we begin to grow $SrIrO_3$ on

the as-prepared buffer layers, a remarkable streak [marked with red square in Fig. 2(c)] could be clearly observed between (00) and (01) diffraction spots. The intensity of this extra secondary diffraction increases as more layers of $SrIrO_3$ were deposited. Meanwhile, we rotated the sample manipulator by 90°, no other diffraction features were seen in the [001] direction, uncovering a (1×2) reconstruction on the surface of the as-grown $SrIrO_3$ films.

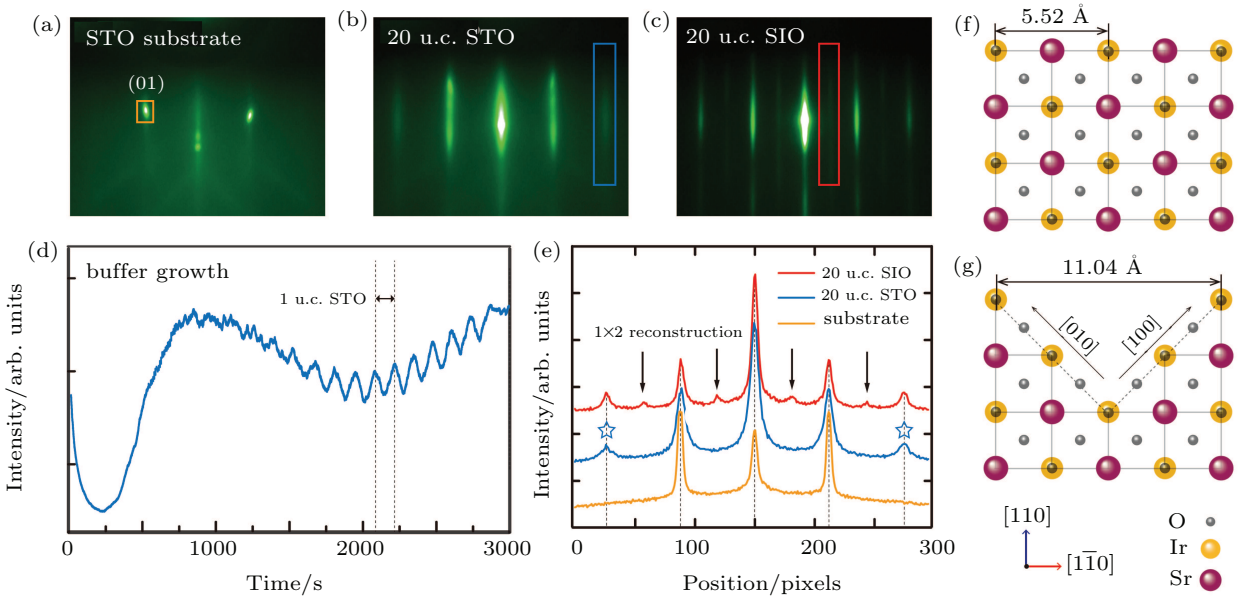


Fig. 2. (color online) RHEED pattern before deposition (a), after depositing buffer layers (b), and after depositing 20 u.c. $SrIrO_3$ films (c). (d) Diffraction intensity oscillation of buffer layers. (e) Comparison of integration curves over different periods. (f) Ideal surface of (110)-$SrIrO_3$. (g) (1×2) reconstruction on the surface of the as-grown $SrIrO_3$ films.

Due to the polarity of the (110) perovskite materials, an infinite dipole moment exists perpendicular to the surface, causing the pristine surface to be unstable and outermost atoms rearranged spontaneously.[20] For (110)-$SrTiO_3$, slight annealing can lead to various types of reconstruction,[21] and the (1×2) reconstruction results from desorption of a large amount of atoms on the Ti-terminated surface.[22] Despite the non-negligible instability in (110)-$SrTiO_3$, the periodic oscillation curve [Fig. 2(d)] sufficiently declared the high crystalline quality of the buffer layers without any unfavorable reconstruction. However, there was no noticeable oscillation during the deposition of (110)-$SrIrO_3$ films, which is likely to be the cause of the surface reconfiguration with the distance between adjacent Ir atoms expanding from 5.52 Å to 11.04 Å [Figs. 2(f)–2(g)]. Periodic loss of considerable atoms leads to the appearance of vertical microfacets (100)/(010) IrO_2 on the surface. Hence, compared to (110)-$SrTiO_3$, (110)-$SrIrO_3$ seems more difficult to obtain an ideal surface. What is more, the atomic force microscopy (AFM) image indicates the mean roughness of (110)-$SrIrO_3$ films over an arbitrarily selected 2 μm segment is about 0.5 nm [Figs. 3(a)–3(b)]. Such a value is nearly equivalent to the thickness of 2-u.c. atoms, exactly in line with the (1×2) reconstruction result.

In order to investigate the lattice structure of the samples, we next conducted an *ex situ* XRD test. As seen in Fig. 3(c), apart from the diffraction peaks (green circles) of the substrate corresponding to (110) and (220) planes, there are very distinct diffraction peaks (green triangles) of the epitaxial films on the left side without any other miscellaneous peaks, which implied excellent single crystal orientation. Using the Bragg diffraction formula, we can calculate the lattice constant of 5.52 Å in the [1$\bar{1}$0] direction of $SrIrO_3$ films. Moreover, the rocking curve measurement for the (220) peak is shown in the inset of Fig. 3(c). The full width at half maximum obtained after fitting by Gaussian is about 0.06°, which is comparable with 0.05° of the substrate, indicating the good crystal quality of our epitaxially grown films.

A comparison between (001)-$SrIrO_3$ and (110)-$SrIrO_3$ on electrical transport is shown in Fig. 3(d), from which the slope for resistivity versus temperature of the (110) oriented film experienced a transition from negative to positive, reaching a minimum value around 170 K. This upturned resistivity feature can be frequently observed not only in $SrIrO_3$ thin films[23–27] but also in $SrIrO_3$ crystals,[28] possibly derived from weak localization effects[29] or pseudogap formation.[28] The ratio of ρ_{min} and ρ_{max} in (110)-$SrIrO_3$ is approximately equal to 0.9, such a narrow resistance range implies semimetallic properties.[26,30] When the temperature drops to 2 K, the resistivity of (110)-$SrIrO_3$ is only 55% of the (001)-oriented counterpart and hits 70% at 300 K. Therefore, (110)-$SrIrO_3$ indeed conducts more pronounced semimetallic behavior than (001)-$SrIrO_3$ throughout the temperature range, which may result from the unique surface states protected by lattice symmetry of the (110)-oriented films.

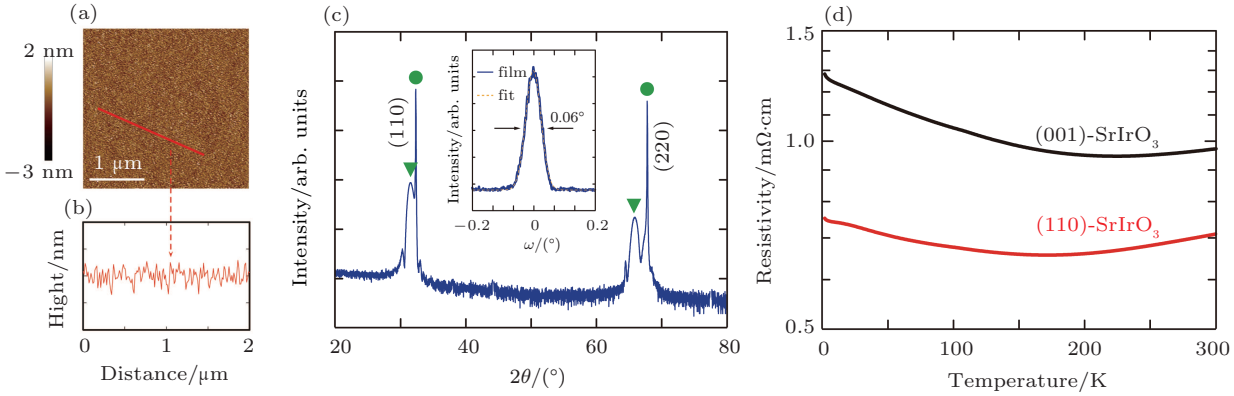


Fig. 3. (color online) (a) AFM image of $SrIrO_3$ film. (b) The mean roughness over 2 μm is about 0.5 nm. (c) XRD pattern of $SrIrO_3$ film. (d) T-dependent ρ curves for (001)-$SrIrO_3$ and (110)-$SrIrO_3$.

The *in situ* RHEED patterns combined with *ex situ* XRD tests complementarily reveal the high-quality crystallization of hetero-epitaxy (110)-$SrIrO_3$ films. However, the evolution of RHEED fringes also reveals surface reconstruction in the $[1\bar{1}0]$ direction. Even if we tried to anneal these samples at 650 °C or higher temperatures for 30 minutes under an ozone pressure of 2.5×10^{-6} Torr, or reduced the deposition rate by adjusting the temperature of each source synchronously, this phenomenon still exists. In addition, the (110)- and (001)-oriented epitaxial films suffer from different stress from the substrate, which possibly affects the interaction between SOC and electron-correlation, may lead to new physical phenomena.

4. Conclusion

In summary, we have successfully synthesized high-quality (110)-$SrIrO_3$ thin films with effective polar buffer layers utilizing MBE for the first time. The precise orientation and excellent crystallinity have been confirmed by both RHEED monitoring and XRD test. A (1×2) reconstitution was observed simultaneously, which is originating from an increased lattice constant in the $[1\bar{1}0]$ direction. Compared with (001)-$SrIrO_3$, (110)-$SrIrO_3$ displays more obvious semimetallic behavior below 300 K, in good agreement with the theoretical prediction. Our research provides a valuable reference for the quality enhancement of polar oxide films. More importantly, it lays a solid foundation for the research on mutual competition between SOC and strong electron-correlation in perovskite iridates. More electronic structure investigations such as ARPES studies are expected to confirm the hypothetical non-trivial topological states.

References

[1] Tian Z M, Kohama Y, Tomita T, Ishizuka H, Hsieh T H, Ishikawa J J, Kindo K, Balents L and Nakatsuji S 2016 *Nat. Phys.* **12** 134

[2] Anderson T J, Ryu S, Zhou H, Xie L, Podkaminer J P, Ma Y, Irwin J, Pan X Q, Rzchowski M S and Eom C B 2016 *Appl. Phys. Lett.* **108** 151604

[3] Groenendijk D J, Manca N, Mattoni G, Kootstra L, Gariglio S, Huang Y, Heumen E and Caviglia A D 2016 *Appl. Phys. Lett.* **109** 041906

[4] Boseggia S, Springell R, Walker H C, Rønnow H M, Rüegg C, Okabe H, Isobe M, Perry R S, Collins S P and McMorrow D F 2013 *Phys. Rev. Lett.* **110** 117207

[5] Takayama T, Kato A, Dinnebier R, Nuss J, Kono H, Veiga L S I, Fabbris G, Haskel D and Takagi H 2015 *Phys. Rev. Lett.* **114** 077202

[6] Groenendijk D J, Autieri C, Girovsky J, Martinez-Velarte M C, Manca N, Mattoni G, Monteiro A M R V L, Gauquelin N, Verbeeck J, Otte A F, Gabay M, Picozzi S and Caviglia A D 2017 *Phys. Rev. Lett.* **119** 256403

[7] Schütz P, Di Sante D, Dudy L, Gabel J, Stübinger M, Kamp M, Huang Y, Capone M, Husanu M A, Strocov V N, Sangiovanni G, Sing M and Claessen R 2017 *Phys. Rev. Lett.* **119** 256404

[8] Nie Y F, King P D C, Kim C H, Uchida M, Wei H I, Faeth B D, Ruf J P, Ruff J P C, Xie L, Pan X, Fennie C J, Schlom D G and Shen K M 2015 *Phys. Rev. Lett.* **114** 016401

[9] Liu Z T, Li M Y, Li Q F, Liu J S, Li W, Yang H F, Yao Q, Fan C C, Wan X G, Wang Z and Shen D W 2016 *Sci. Rep.* **6** 30309

[10] Carter J M, Shankar V V, Zeb M A and Kee H Y 2012 *Phys. Rev. B* **85** 115105

[11] Zeb M A and Kee H Y 2012 *Phys. Rev. B* **86** 085149

[12] Chen Y G, Kim H S and Kee H Y 2016 *Phys. Rev. B* **93** 155140

[13] Fujioka J, Okawa T, Yamamoto A and Tokura Y 2017 *Phys. Rev. B* **95** 121102

[14] Biswas A and Jeong Y H 2017 *Curr. Appl. Phys.* **17** 605

[15] Chen Y G, Lu Y M and Kee H Y 2015 *Nat. Commun.* **6** 6593

[16] Groenendijk D J, Manca N, Mattoni G, Kootstra L, Gariglio S, Huang Y, Heumen E V and Caviglia A D 2016 *Appl. Phys. Lett.* **109** 041906

[17] Smith E H, Ihlefeld J F, Heikes C A, Paik H, Nie Y F, Adamo C, Heeg T, Liu Z K and Schlom D G 2017 *Phys. Rev. Mater.* **1** 023403

[18] Savoia A, Paparo D, Perna P, Ristic Z, Salluzzo M, Granozio F M, Di Uccio U S, Richter C, Thiel S, Mannhart J and Marrucci L 2009 *Phys. Rev. B* **80** 075110

[19] Yang H F, Liu Z T, Fan C C, Yao Q, Xiang P, Zhang K L, Li M Y, Liu J S and Shen D W 2016 *AIP Adv.* **6** 085115

[20] Kotomin E A, Heifets E, Dorfman S, Fuks D, Gordon A and Maier J 2004 *Surf. Sci.* **566** 231

[21] Brunen J and Zegenhagen J 1997 *Surf. Sci.* **389** 349

[22] Gunhold A, Beuermann L, Gömann K, Borchardt G, Kempter V, Maus-Friedrichs W, Piskunov S, Kotomin E A and Dorfman S 2003 *Surf. Interface Anal.* **35** 998

[23] Biswas A, Kim K S and Jeong Y H 2014 *J. Appl. Phys.* **116** 213704

[24] Kim Y K, Sumi A, Takahashi K, Yokoyama S, Ito S, Watanabe T, Akiyama K, Kaneko S, Saito K and Funakubo H 2005 *Jpn. J. Appl. Phys.* **45** L36

[25] Moon S J 2014 *J. Korean Phys. Soc.* **64** 1174

[26] Zhang L Y, Liang Q F, Xiong Y, Zhang B B, Gao L, Li H D, Chen Y B, Zhou J, Zhang S T, Gu Z B, Yao S H, Wang Z M, Lin Y and Chen Y F 2015 *Phys. Rev. B* **91** 035110

[27] Gruenewald J H, Nichols J, Terzic J, Cao G, Brill J W and Seo S S A 2014 *J. Mater. Res.* **29** 2491

[28] Zhao J G, Yang L X, Yu Y, Li F Y, Yu R C, Fang Z, Chen L C and Jin C Q 2008 *J. Appl. Phys.* **103** 103706

[29] Wu F X, Zhou J, Zhang L Y, Chen Y B, Zhang S T, Gu Z B, Yao S H and Chen Y F 2013 *J. Phys.: Condens. Matter* **25** 125604

[30] Biswas A, Kim K S and Jeong Y H 2016 *J. Magn. Magn. Mater.* **400** 36